



ELSEVIER

Contents lists available at ScienceDirect

Journal of Magnetism and Magnetic Materials

journal homepage: www.elsevier.com/locate/jmmm

Thermoelectric, band structure, chemical bonding and dispersion of optical constants of new metal chalcogenides $Ba_4CuGa_5Q_{12}$ (Q=S, Se)

A.H. Reshak^{a,b}, Sikander Azam^{a,*}^a New Technologies – Research Center, University of West Bohemia, Univerzitni 8, 306 14 Pilsen, Czech Republic^b Center of Excellence Geopolymer and Green Technology, School of Material Engineering, University Malaysia Perlis, 01007 Kangar, Perlis, Malaysia

ARTICLE INFO

Article history:

Received 9 November 2013

Received in revised form

24 January 2014

Available online 14 February 2014

Keywords:

Electronic structure

Fermi surface

Dispersion of optical constant

Thermoelectric property

ABSTRACT

The electronic structure and dispersion of optical constants of the $Ba_4CuGa_5S_{12}$ and $Ba_4CuGa_5Se_{12}$ compounds were calculated by the first-principles full-potential linearized augmented plane wave (FP-LAPW) method. We employed the local density approximation (LDA), generalized gradient approximation (GGA) and Engel–Vosko GGA (EVGGA) to calculate the electronic structures, Fermi surface, thermoelectric, chemical bonding and dispersion of optical constants of these compounds. By investigating the influence of replacing S by Se, it has been found that the charge density around ‘Ga’ is greater in $Ba_4CuGa_5Se_{12}$ than $Ba_4CuGa_5S_{12}$. Fermi surface of $Ba_4CuGa_5S_{12}$ consists of an electronic sheet only because there is no empty region while $Ba_4CuGa_5Se_{12}$ contains both holes and electronic sheets because this compound contains both empty and shaded region. As we replace S by Se the heights of the peaks decreases as a result the reflectivity also decreases. It is noticed that the reflectivity is over 68% (60%) for $Ba_4CuGa_5S_{12}$ ($Ba_4CuGa_5Se_{12}$) compounds within the energy range studied. This implies that the material will serve as a good reflector. By replacing S by Se the figure of merit values increases from 0.97 to 1.0, which shows the good thermoelectric behavior of both compounds.

© 2014 Elsevier B.V. All rights reserved.

1. Introduction

Nonlinear optical (NLO) devices for frequency transformation of high-power laser radiation require highly efficient NLO materials [1–5]. LiB_3O_5 , [6] β - BaB_2O_4 , [7–9] $KTiPO_4$, [10] and $LiNbO_3$ [11,12] are the oxide-based materials, which are renowned for their outstanding NLO properties in the UV–vis range. Though, the provision of a wide transparency range, an adequate birefringence, high laser damage threshold and a large nonlinear susceptibility confines the number materials appropriate for application in the IR region [4].

The chalcopyrite semiconductors, as $CdGeAs_2$, $Ag-GaSe_2$, $ZnGeP_2$ and $AgGaS_2$ [13–26] are the current commercial infrared NLO materials. Recently, it has been reported that many newly structural chalcogenide- and pnictide-based materials have the promising infrared NLO properties.

The polar units of building block anions, chains, or layers [27–41] contained these structures are assumed to be most

important to their high second harmonic generation (SHG) responses. For instance, the thick slabs in β - $K_2Hg_3Ge_2S_8$, [35] the pucker layers in $CaZnOS$ [36] and $Na_2Ge_2Se_5$, [37] or the hexagonal layers in Li_2CdGeS_4 [38] all have tetrahedra leaning in the same direction. In the same way, $Ba_3CsGa_5Se_{10}Cl_{12}$ compound displayed the SHG intensity 100 times more than that of $AgGaS_2$ by using an incident laser at 2.05 μm . The structure of $Ba_3CsGa_5Se_{10}Cl_{12}$ compound holds the pseudo layers consisting of leaning supertertaedra of Ga_4Se_{10} [41]. Besides this the glassy materials having excellent mechanical properties and structures composed of polar chains such as $[P_2Se_6]^{2-}$ and $[PSe_6]^{1-}$ also have inspiring NLO properties [30,31]. In the beginning of 2013 Shu-Ming Kuo et al. [42] represent a series of novel infrared NLO materials of $Ba_4CuGa_5Q_{12}$ (Q=S, $S_{0.75}Se_{0.25}$, Se), which are considered as the first members discovered in the quaternary $Ba/Cu/Ga/Q$ (Q=S, Se) systems.

In this work, the full-potential linearized augmented plane-wave (FP-LAPW) method based on the first-principles density functional theory (DFT) with in the local density approximation (LDA), generalized gradient approximation (GGA) and Engel Vosko generalized gradient approximation (EVGGA) exchange potential approximation are used to calculate accurately the electronic

* Corresponding author. Tel.: +420 775928620; fax: +420 386361219.

E-mail addresses: sikander.physicst@gmail.com, sikandar_hu@yahoo.com (S. Azam).

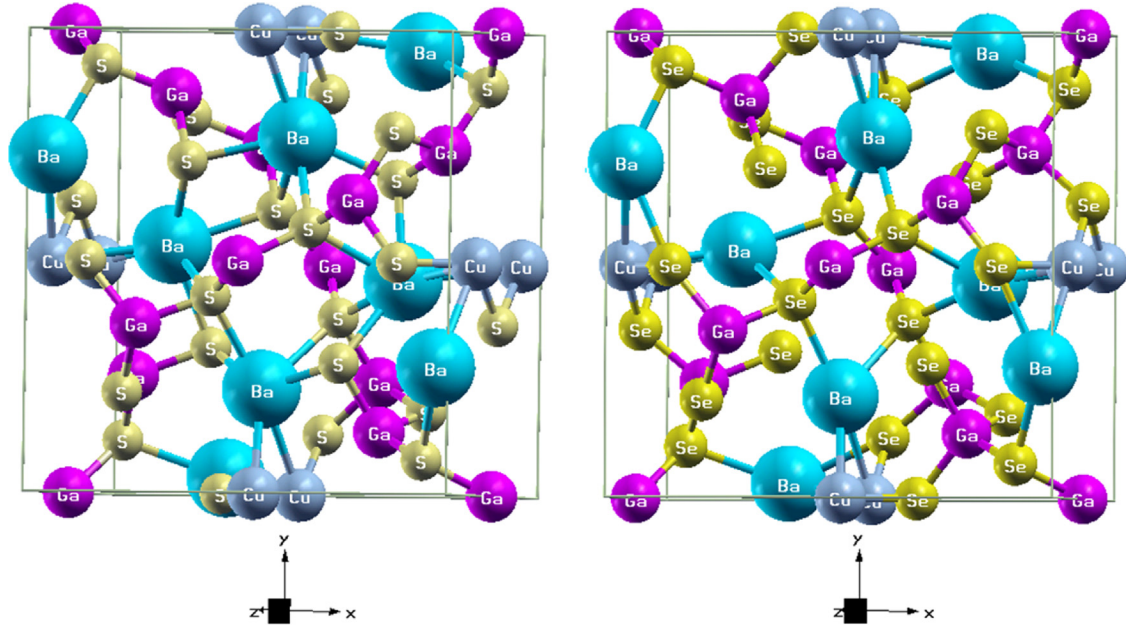


Fig. 1. Unit cell structure for $\text{Ba}_4\text{CuGa}_5\text{S}_{12}$ and $\text{Ba}_4\text{CuGa}_5\text{Se}_{12}$ compounds.

Table 1
Atomic coordinates for $\text{Ba}_4\text{CuGa}_5\text{S}_{12}$ compound.

Atom	X exp.	X opt.*	Y exp.	Y. opt.*	Z exp.	Z opt.*
Ba1	0.21665(3)	0.22657	0.53251(3)	0.53796	0.45668(7)	0.45577
Ga1	0.13519(4)	0.13571	0.24754(4)	0.25426	0.44819(10)	0.43488
Ga2	0	0	0	0.0	0.5	0.5
Cu1	0	0	0.5	0.5	0.7071(3)	0.7110
S1	0.0052(1)	0.9996	0.3622(1)	0.3677	0.4592(2)	0.4610
S2	0.0799(1)	0.0751	0.1078(1)	0.1156	0.2693(2)	0.2601
S3	0.2813(1)	0.2828	0.3069(1)	0.3175	0.2835(21)	0.2762
Atomic coordinates for $\text{Ba}_4\text{CuGa}_5\text{Se}_{12}$ compound						
Ba1	0.21300(4)	0.21937	0.52769(4)	0.53534	0.45598(9)	0.44126
Ga1	0.13779(6)	0.13987	0.24555(6)	0.24959	0.44539(15)	0.41741
Ga2	0	0	0	0.0	0.5	0.5
Cu1	0	0	0.5	0.5	0.7067(4)	0.6960
Se1	0.0051(1)	0.0052	0.3617(1)	0.3645	0.4592(1)	0.4466
Se2	0.0811(1)	0.07383	0.1056(1)	0.1140	0.2588(1)	0.2305
Se3	0.2867(1)	0.28893	0.3075(1)	0.3170	0.2878(1)	0.2693

* This work.

structure, charge density, optical and thermoelectric properties of the new metal chalcogenides $\text{Ba}_4\text{CuGa}_5\text{Q}_{12}$ ($\text{Q}=\text{S}, \text{Se}$).

The rest of the paper has been divided in four parts. In Section 2, we briefly describe the computational method used in this study. The most relevant results obtained for the electronic and dispersion of optical constants of $\text{Ba}_4\text{CuGa}_5\text{S}_{12}$ and $\text{Ba}_4\text{CuGa}_5\text{Se}_{12}$ compounds are presented and discussed in Section 3. Also the thermoelectric properties were presented in Section 4. Finally, we summarize the main conclusions in Section 5.

2. Methodology

The self-consistent calculations were carried out using Wien2k code [43] based on the full-potential linear augmented plane wave method. LDA, GGA and EVGGA [44–46], were used to treat the exchange correlation potential by solving Kohn–Sham equations, in order to estimate the sensitivity of the results to exchange correlation. We have considered the tetragonal structure of $\text{Ba}_4\text{CuGa}_5\text{S}_{12}$ and $\text{Ba}_4\text{CuGa}_5\text{Se}_{12}$ compounds [42] (see Fig. 1). The optimized atomic positions in comparison with the experimental one [42] are shown in

Table 1. The sphere radii used were 2.0 a.u. for Ba, Cu, Ga and S/Se respectively. The Brillouin zone integration was carried out by using the modified tetrahedron method [47]. Well converged solutions were obtained with $R_{MT}K_{max}=7.0$ (where R_{MT} is the smallest of the muffin-tin radii and K_{max} is the plane wave cut-off) and k-point sampling was checked.

For the calculation of the optical properties, which usually requires a dense mesh of uniformly distributed k -points, the Brillouin zone integration was performed using the tetrahedron method with 200 k -points in the irreducible part of the Brillouin zone without broadening. The dielectric function $\epsilon(\omega)$ is known to describe the optical response of the medium at all photon energies. In metals, there are two contributions to dielectric function arising from the interband and intraband transitions. The interband transitions can be further split into direct and indirect transitions. However, both the intraband and indirect interband transitions involve phonon in order to account for the momentum transfer. The calculated direct interband contribution to the imaginary part of the dielectric function, $\epsilon(\omega)$, is calculated by summing transitions from occupied to unoccupied states (with fixed k) over the Brillouin zone, weighted with the appropriate matrix elements giving the probability for the transition. Specifically, in this study, the imaginary part of the dielectric function $\epsilon(\omega)$ is given as in Ref. [48]

$$\epsilon_2^{ij}(\omega) = \frac{4\pi^2 e^2}{Vm^2\omega^2} \sum_{kn\sigma} \langle kn\sigma | p_i | kn'\sigma \rangle \langle kn'\sigma | p_j | kn\sigma \rangle \times f_{kn}(1-f_{kn'})\sigma(E_{kn'} - E_{kn} - \hbar\omega) \quad (1)$$

where e is the electron charge and m is the mass, ω is the frequency of the incoming electromagnetic radiation, V is the volume of the unit cell, $(p_x, p_y, p_z)=p$ is the momentum operator $|kn\sigma\rangle$ the crystal wave function, corresponding to eigenvalue E_{kn} with crystal momentum k and spin σ . Finally, f_{kn} is the Fermi distribution function ensuring that only transitions from occupied to unoccupied states are counted, and $\sigma(E_{kn'} - E_{kn} - \omega)$ is the condition for total energy conservation.

Since the investigated compound has the metallic nature thus we include the intraband transitions. Therefore both of the intraband and inter-band transitions contribute

$$\epsilon_2(\omega) = \epsilon_{2inter}(\omega) + \epsilon_{2intra}(\omega) \quad (2)$$

where

$$\varepsilon_{2intra}^{xx}(\omega) = \frac{\omega_p^{xx} \tau}{\omega(1 + \omega^2 \tau^2)} \quad (3)$$

$$\varepsilon_{2intra}^{zz}(\omega) = \frac{\omega_p^{zz} \tau}{\omega(1 + \omega^2 \tau^2)} \quad (4)$$

where τ and ω_p [49] are the mean free time and mean frequency amongst the collisions.

$$\omega_p^2 = \frac{8\pi}{3} \sum_{kn} \vartheta_{kn}^2 \delta(\varepsilon_{kn}) \quad (6)$$

As ε_{kn} is $E_n(k) - E_F$ and ϑ_{kn} is the velocity of electron.

The BoltzTraP code was then employed to calculate the thermoelectric properties based on the analytical expressions of the electronic bands. The constant relaxation time approximation and the rigid band approximation were used in the calculations. In order to better understand the temperature and chemical potential dependent thermoelectric properties, we performed calculations that are based on the semi-classical electronic transport theory and the empirical lattice thermal conductivity model. We have calculated Seebeck coefficients, thermal conductivity, electrical conductivity and figure of merit.

3. Results and discussion

3.1. Electronic structure

The calculated electronic energy band structure of $\text{Ba}_4\text{CuGa}_5\text{S}_{12}$ ($\text{Ba}_4\text{CuGa}_5\text{Se}_{12}$) compounds along the high symmetry directions of the tetragonal Brillouin zone is displayed in Fig. 2. It shows clearly the metallic nature of both compounds. The Ga-s band between -0.2 and 1.0 eV with S/Se-p bands crossing the Fermi level to form humps across the Fermi level between the Γ and X (Z and M) points for $\text{Ba}_4\text{CuGa}_5\text{S}_{12}$ ($\text{Ba}_4\text{CuGa}_5\text{Se}_{12}$) compounds. The width of the valence band is about 18.0 eV. The small Se-d state presence in the conduction band is seen only around the highest portion. In the energy range between -18.0 and -5.0 eV, S-p hybridizes with S-s, Ga-s, Cu-s with S/Se-p and Se-s with Ga-s states. At 7.0 eV Cu-p hybridized with Se-d state. The lowest broad band lying between 10.0 and 12.0 eV below the Fermi level is predominantly due to Ba-s and Se-d states. The electron distribution in an energy spectrum is described by the density of states (DOS).

In order to explain the nature of the electronic band structures, we have calculated the total and partial density of states (TDOS and PDOS) for these compounds. These are displayed in Fig. 3. As we replace S by Se, whole structures are shifted towards higher energies by around 0.7 eV. The total DOS has prominent structures at -18.0 up to -14.0 eV, -9.0 till 3.5 eV and at 0.0 up to 5.0 eV. The Ga-s bands show high dispersion in the electronic band structure around the Fermi level which is probably responsible for the metallic properties of the compound. The S/Se-s and Cu-s partial DOS in the middle panels of Fig. 3, show that there is some hybridization between S/Se-s and Cu-s above E_F . The most significant contributions to the total DOS come in the region between -18.0 to -15.0 eV arise from predominantly Ba-p and Ga-d states contributions.

As electrons near the Fermi surface are involved in the configuration of the conducting state, it is significant to understand their nature. The total, atomic, and orbital decomposed partial DOSs at the Fermi level, $N(E_F)$ has been calculated. The total DOS at Fermi level $N(E_F)$ for $\text{Ba}_4\text{CuGa}_5\text{S}_{12}$ ($\text{Ba}_4\text{CuGa}_5\text{Se}_{12}$) is 16.512 (13.260) (states/eV unit cell). The metallic character of the two compounds is clearly seen from the finite DOS at the Fermi level. It is clear from

Fig. 3a that the $N(E_F)$ is the highest for $\text{Ba}_4\text{CuGa}_5\text{S}_{12}$ as compared to $\text{Ba}_4\text{CuGa}_5\text{Se}_{12}$, which shows that $\text{Ba}_4\text{CuGa}_5\text{S}_{12}$ is more metallic than $\text{Ba}_4\text{CuGa}_5\text{Se}_{12}$. The electronic specific heat coefficient (γ), which is function of $N(E_F)$ can be calculated using the expression $\gamma = 1/3\pi^2 N(E_F) K_B^2$, where K_B is the Boltzmann constant. The calculated $N(E_F)$ enables us to obtain the bare electronic specific heat coefficient, which is found to be equal to 2.864 (2.300) mJ/mol-K² for $\text{Ba}_4\text{CuGa}_5\text{S}_{12}$ ($\text{Ba}_4\text{CuGa}_5\text{Se}_{12}$), respectively.

3.2. Electronic charge density

Electronic charge density denotes the nature of the bond character. In order to predict the chemical bonding and also the charge transfer in $\text{Ba}_4\text{CuGa}_5\text{S}_{12}$ and $\text{Ba}_4\text{CuGa}_5\text{Se}_{12}$ compounds, the charge-density behaviors in 2D are calculated in the (101) plane and displayed in Fig. 4. The result shows that the substitution of the S by Se leads to redistribution of electron charge density i.e. the bond distances increase. As when an atom is interchanged by the other atom the VSCC (valence shell charge carrier) properties changes [50]. By investigating the influence of replacing S by Se in $\text{Ba}_4\text{CuGa}_5\text{S}_{12}$ and $\text{Ba}_4\text{CuGa}_5\text{Se}_{12}$ compounds, it has been found that the charge density around 'Ga' is greater in $\text{Ba}_4\text{CuGa}_5\text{Se}_{12}$ than $\text{Ba}_4\text{CuGa}_5\text{S}_{12}$. From the calculated electron density it is clear that Ga and S/Se form partial covalent and partial ionic bond, while Cu and Ba form ionic bonding. We have also calculated the bond lengths and the bond angles which show good agreement with the experimental work [42] (see Table 2).

3.3. Fermi surface

Fig. 5 illustrates the near-Fermi band structure of $\text{Ba}_4\text{CuGa}_5\text{S}_{12}$ ($\text{Ba}_4\text{CuGa}_5\text{Se}_{12}$) beside the selected high-symmetry lines in the first Brillouin zone of the tetragonal crystal. It is seen that the Fermi level is crossed by S/Se-p and Ba-s bands, which specifies that the electrical conductivity of this phase should be metallic. The electrons closest to the Fermi level are responsible for conductivity; the electronic structure of any metallic material is understandable from the Fermi surface (FS). We have shown the Fermi surface of $\text{Ba}_4\text{CuGa}_5\text{S}_{12}$ ($\text{Ba}_4\text{CuGa}_5\text{Se}_{12}$), in order to get a better report of the states crossing the Fermi level. The shaded region in the FS shows the electronic sheets and the empty space shows the holes. The FS of $\text{Ba}_4\text{CuGa}_5\text{S}_{12}$ consists of an electronic sheet only because there is no empty region while $\text{Ba}_4\text{CuGa}_5\text{Se}_{12}$ contains both holes and electronic sheets because this compound contains both empty and shaded region [51]. There are two bands crossing the E_F level in both investigated compound. The relevant Fermi surface structures ensuing from these two bands are depicted in Fig. 5, along with the merged band. The near-Fermi bands display an intricate "mixed" character: concurrently with quasi-flat bands along Γ -X (Z-M) for $\text{Ba}_4\text{CuGa}_5\text{S}_{12}$ ($\text{Ba}_4\text{CuGa}_5\text{Se}_{12}$) compounds, a series of high dispersive bands intersects the Fermi level. Fermi surface defines various electrons in the system, whose topology is instantly related to the transport features of materials, such as electrical conductivity.

3.4. Dispersion of optical constants

In Fig. 6, we have displayed the calculated imaginary part of the dielectric function for $\text{Ba}_4\text{CuGa}_5\text{S}_{12}$ ($\text{Ba}_4\text{CuGa}_5\text{Se}_{12}$) as a function of the photon energy from 0.0 to 14.0 eV. The dielectric function ($\varepsilon(\omega) = \varepsilon_1(\omega) + i\varepsilon_2(\omega)$) spectra will help in accounting for the optical transitions in $\text{Ba}_4\text{CuGa}_5\text{S}_{12}$ ($\text{Ba}_4\text{CuGa}_5\text{Se}_{12}$). The imaginary part of the dielectric function, $\varepsilon_2(\omega)$, was calculated using Eq. (1). The calculated dielectric functions $\varepsilon_2^{xx}(\omega)$ and $\varepsilon_2^{zz}(\omega)$ of the investigated compounds using EVGGA are illustrated in Fig. 6a and b. There is a prominent structure in the imaginary part of the

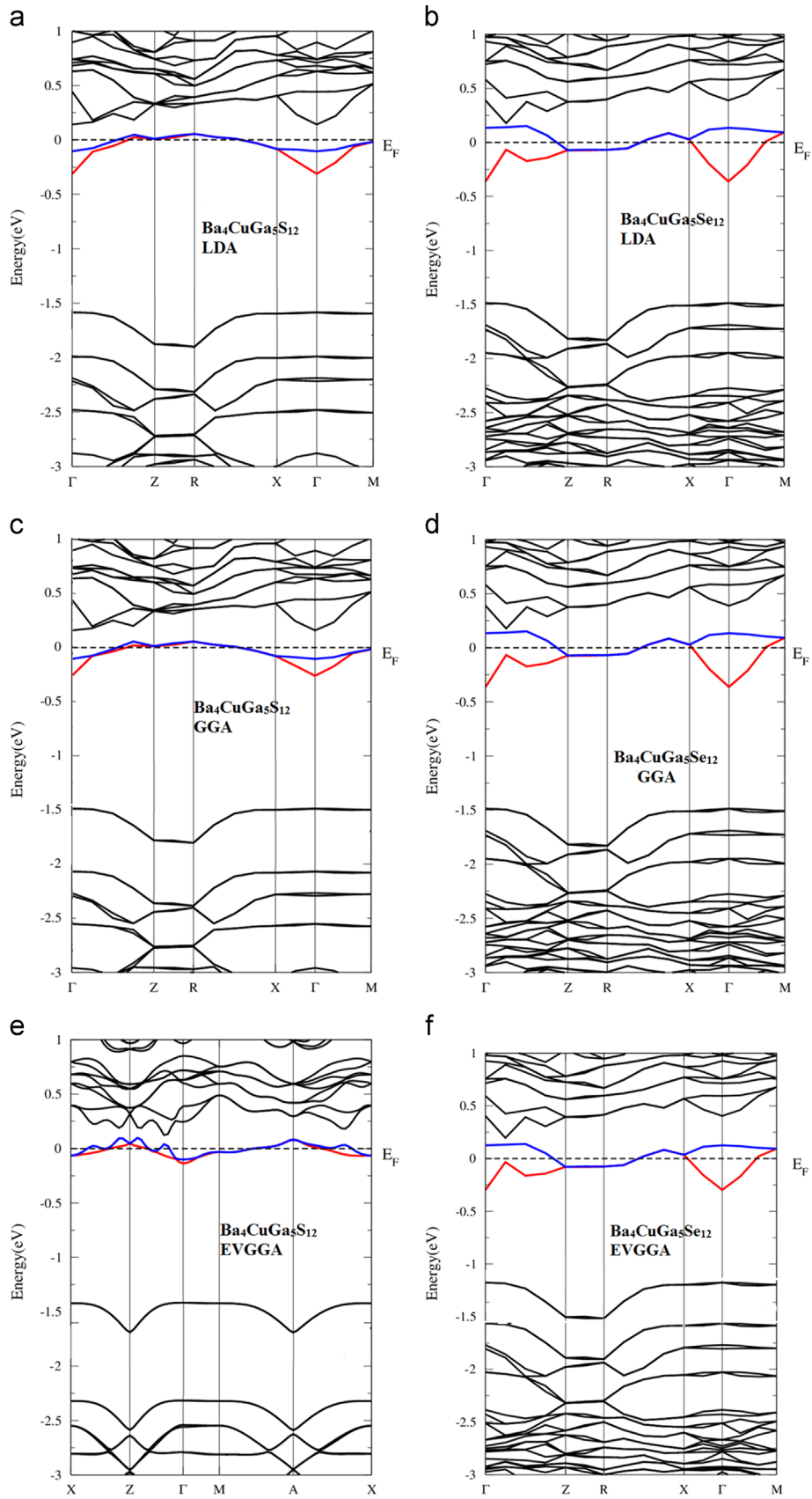


Fig. 2. Calculated band structures for LDA, GGA and EVGGA for $\text{Ba}_4\text{CuGa}_5\text{S}_{12}$ and $\text{Ba}_4\text{CuGa}_5\text{Se}_{12}$ compounds.

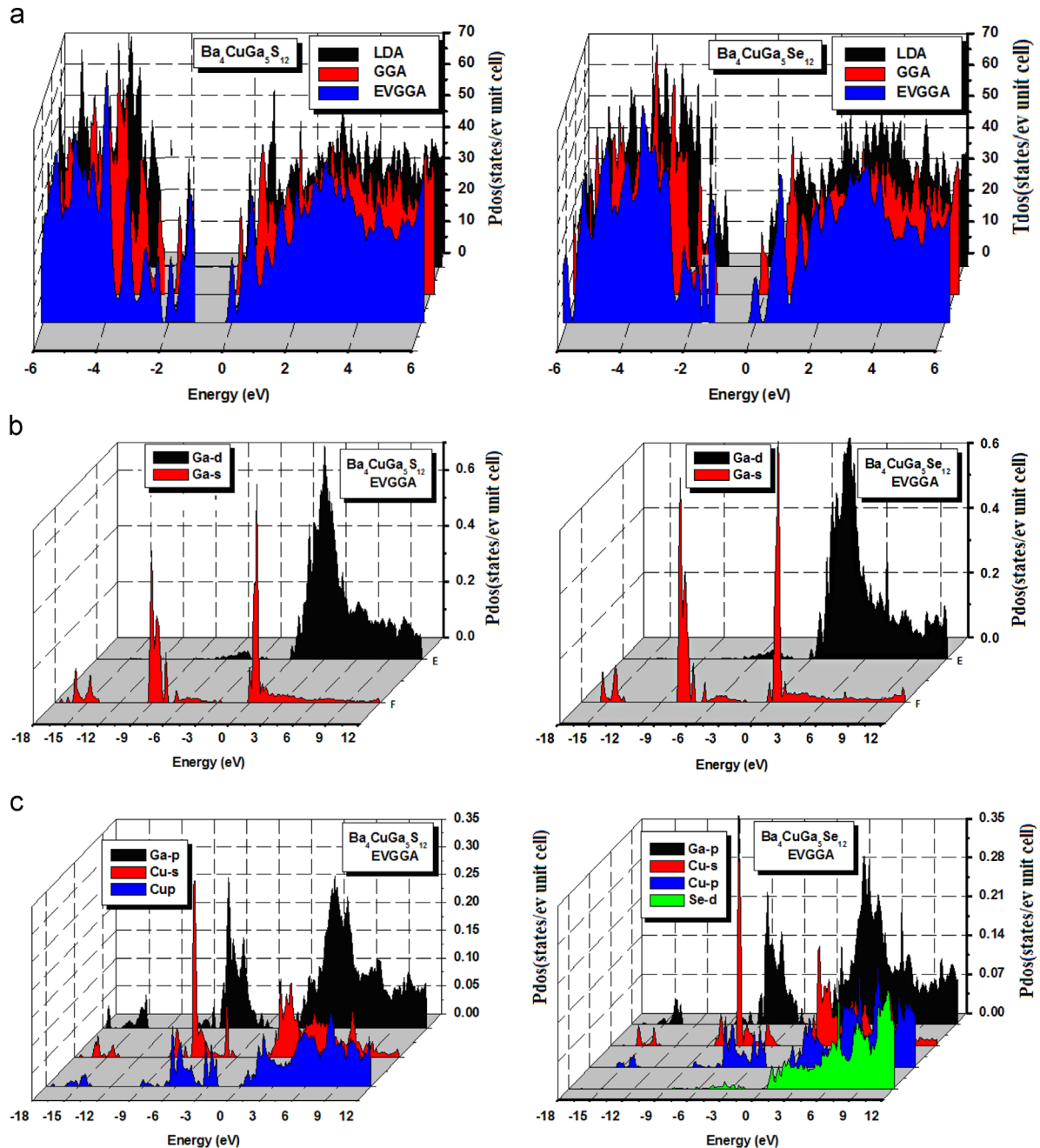


Fig. 3. Calculated total and partial density of state for $\text{Ba}_4\text{CuGa}_5\text{S}_{12}$ and $\text{Ba}_4\text{CuGa}_5\text{Se}_{12}$ compounds (state/eV unit cell).

dielectric function of the compound depicted by peaks around 1.0 eV and from 4.0 eV to 8.0 eV, the decrease in peaks occurs at higher energies. These structures at about 1.0 eV are associated with direct interband transitions. From band structure results, the transitions originate from the occupied S-p bands below the Fermi level to the unoccupied Ba-s states above E_F . This is probably due to strong interband transitions from deeper lying valence bands to unoccupied bands above the Fermi level. As we replace S by Se the heights of the peaks decreases.

Fig. 6c–f, shows the imaginary and real parts of the optical conductivity $\sigma(\omega) = \sigma_1(\omega) + i\sigma_2(\omega)$. In the optical conductivity spectra the peaks can be determined by the electric-dipole transitions between the occupied and unoccupied states. The optical conductivity is related to the frequency-dependent dielectric function $\varepsilon(\omega)$ as $\varepsilon(\omega) = 1 + 4\pi i\sigma(\omega)/\omega$. We can see that the imaginary part of the optical conductivity of $\text{Ba}_4\text{CuGa}_5\text{S}_{12}$ $\text{Ba}_4\text{CuGa}_5\text{Se}_{12}$ is

negative till 6.0 eV and then increasing to positive value (see Fig. 6c and d). The real part of the optical conductivity is illustrated in Fig. 6e and f. In the spectral region 0.0–14.0 eV, there exist four maxima which can be assigned to optical transitions from occupied S-p states to unoccupied Ba-s states. The investigated spectra for the reflectivity are displayed in Fig. 6g and h. It is noticed that the reflectivity is over 68% (60%) $\text{Ba}_4\text{CuGa}_5\text{S}_{12}$ ($\text{Ba}_4\text{CuGa}_5\text{Se}_{12}$) compounds within the energy range studied. This implies that the material will serve as a good reflector.

4. Thermoelectric properties

We have calculated the electrical conductivity, thermal conductivity, Seebeck coefficient and figure of merit (ZT) vs. the chemical potential at constant temperatures for 300 and 600 K.

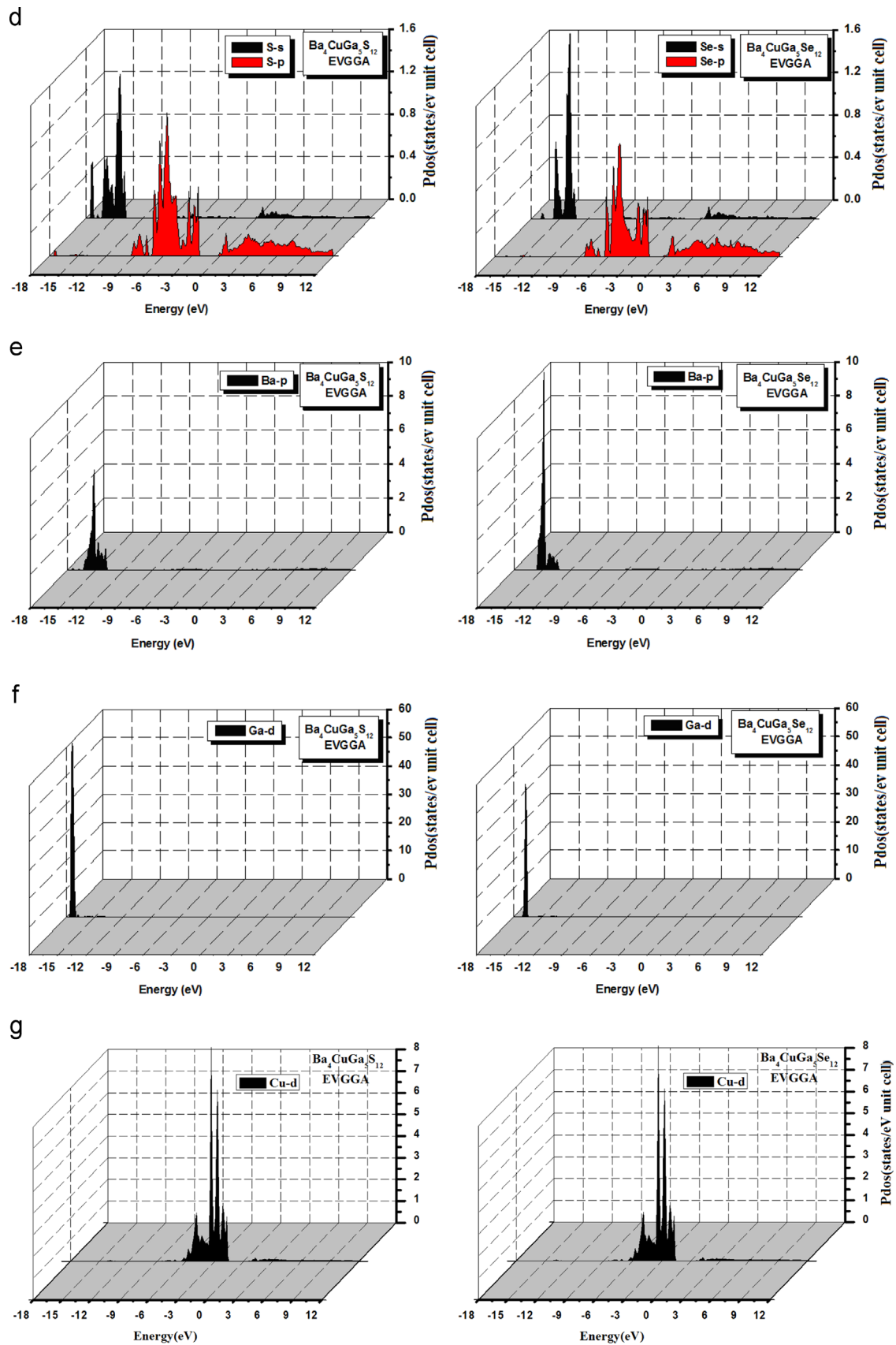


Fig. 3. (continued)

Therefore, S , κ , σ and ZT in the calculated range are dominated by the relaxation time and show a decreasing/increasing trend with increasing temperature.

The electrical conductivity σ was obtained by using the semi-classical Boltzmann theory in conjunction with rigid band and constant relaxation time approximations. All the calculations of

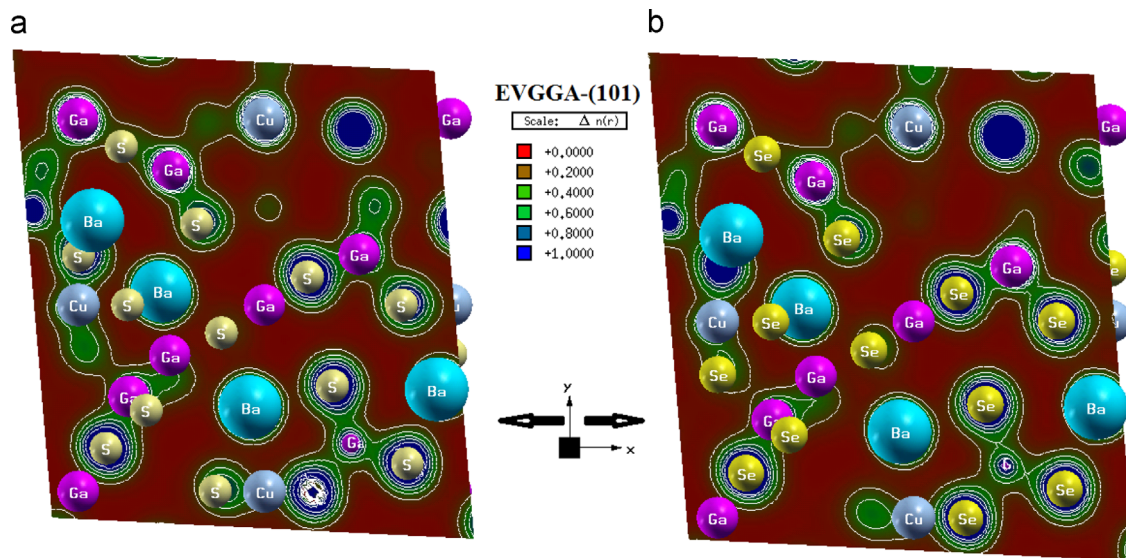


Fig. 4. Calculated electron charge density for $\text{Ba}_4\text{CuGa}_5\text{S}_{12}$ and $\text{Ba}_4\text{CuGa}_5\text{Se}_{12}$ compounds.

Table 2
Selected bond lengths (Å) for $\text{Ba}_4\text{CuGa}_5\text{S}_{12}$ and $\text{Ba}_4\text{CuGa}_5\text{Se}_{12}$ compounds.

Atoms	Exp.	Theory*	Atoms	Exp.	Theory*
Ba(1)–S(3)	3.156(1)	3.174	Ba(1)–Se(3)	3.289(1)	3.327
Ba(1)–S(2)	3.167(2)	3.092	Ba(1)–Se(2)	3.306(1)	3.211
Ba(1)–S(1)	3.207(1)	3.092	Ba(1)–Se(1)	3.344(1)	3.774
Ga(1)–S(1)	2.261(1)	2.315	Ga(1)–Se(2)	2.387(1)	2.385
Ga(1)–S(2)	2.261(2)	2.259	Ga(1)–Se(1)	1.401(1)	2.463
Ga(1)–S(3)	2.276(2)	2.315	Ga(1)–Se(3)	2.396(1)	2.425
Cu(1)–S(1)	2.383(2)	2.336	Cu(1)–Se(1)	2.479(2)	2.458

Exp. Ref. [42].

* This work.

transport properties were implemented in the BoltzTraP package [52], and the necessary crystal structures and eigen-energies for BoltzTraP calculation were obtained from FPLAPW. Fig. 7a and b shows the electrical conductivity spectra, for two constant temperatures 300 and 600 K, from this calculation we get the tendency that the electrical conductivity decreases with increasing temperature and it exhibits metal-like behavior. To calculate the value of σ and k , one has to know the relaxation time τ . The relaxation time illustrates a decreasing drift with increasing the temperature due to the diminution of mobility at the higher temperature. As we see that by increasing the temperature the conductivity of the investigated material decreases.

Metals best suited to thermoelectric applications should therefore possess a high Seebeck coefficient. Unfortunately, most metals show Seebeck coefficients in the order of $10 \mu\text{V}/\text{K}$, which generate efficiencies of only fractions of a percent. The thermoelectric power or Seebeck coefficient (S) can be considered as the heat per carrier over temperature or more simply the entropy per carrier, $S = C/q$ where C is the specific heat and q is the charge of the carrier. For the case of a classical gas each particle has energy of $(3/2)K_B T$ where K_B is the Boltzmann constant. The thermopower is thus approximately K_B/e , where e is the charge of the electron. The expected magnitude for the thermopower of metals, the heat per carrier is essentially a product of the electronic specific heat and the temperature divided by the number of carriers (N),

$$S = \frac{C_{el}}{Q} \approx \frac{K_B}{e} \left(\frac{K_B T}{E_F} \right)$$

where E_F is the Fermi energy (related to the chemical potential of the material) which is basically the energy, such that at $T \approx 0$ all states above this energy are vacant, and all the states below are occupied. The quantity $K_B/e \approx 87 \mu\text{V K}^{-1}$ is a constant, which represents the thermopower of a classical electron gas. Metals have thermopower values much less than $87 \mu\text{V K}^{-1}$.

In a measurement of the Seebeck effect, what is actually measured is the difference in the Seebeck coefficients of the two temperatures. For optimized $\text{Ba}_4\text{CuGa}_5\text{S}_{12}$ ($\text{Ba}_4\text{CuGa}_5\text{Se}_{12}$) compounds we calculated the Seebeck coefficient as shown in Fig. 7c and d, as the temperature increases from 300 K to 600 K the Seebeck coefficient decreases for high temperatures in both compounds. The negative Seebeck coefficients values signify that electron-type carriers dominate the thermoelectric transport in these materials.

The T-dependent thermal conductivity of $\text{Ba}_4\text{CuGa}_5\text{S}_{12}$ ($\text{Ba}_4\text{CuGa}_5\text{Se}_{12}$) for two constant temperature are displayed in Fig. 7e and f. For conventional metals and semimetals, the total thermal conductivity (κ_{tot}) can be expressed as a sum of lattice (κ_L) and electronic (κ_e) terms: $\kappa_{tot} = \kappa_L + \kappa_e$. According to Fig. 7e and f, the thermal conductivity for optimized $\text{Ba}_4\text{CuGa}_5\text{S}_{12}$ compound, there is a decrease in the thermal conductivity spectra as we change the temperature from 300 K to 600 K but the situation in the $\text{Ba}_4\text{CuGa}_5\text{Se}_{12}$ compound is different i.e. there is increase in the spectra as we change the temperature from 300 K to 600 K.

The figure of merit (ZT) value that exceeds unity is essential for practical use as thermoelectric generator or Peltier cooler. For metallic systems, on the assumption that the phononic thermal conductivity $\kappa_{ph} = 0$. A number of compounds have reached values above $ZT = 1$ at high T [39]. In Fig. 7g and h we illustrate the dimensionless figure of merit $ZT = (S^2 \sigma / \kappa) T$ for the investigated compounds as a function of temperature. The calculated figure of merit vs. chemical potential has been shown in Fig. 7g and h. This is the most important quantity for measuring transport properties. The calculated value of dimensionless also shows significant value for $\text{Ba}_4\text{CuGa}_5\text{S}_{12}$ ($\text{Ba}_4\text{CuGa}_5\text{S}_{12}$) is 0.97 (1.0) for n-type at 300 K.

We have also calculated the electrical conductivity, thermal conductivity, Seebeck coefficient and figure of merit (ZT) vs. the various temperatures. The calculated temperature-dependent average electrical conductivity for variable temperature for $\text{Ba}_4\text{CuGa}_5\text{S}_{12}$ and $\text{Ba}_4\text{CuGa}_5\text{Se}_{12}$ is plotted in Fig. 8a. The temperature characteristic of electrical conductivity for $\text{Ba}_4\text{CuGa}_5\text{S}_{12}$ and $\text{Ba}_4\text{CuGa}_5\text{Se}_{12}$ compounds exhibits the different features in

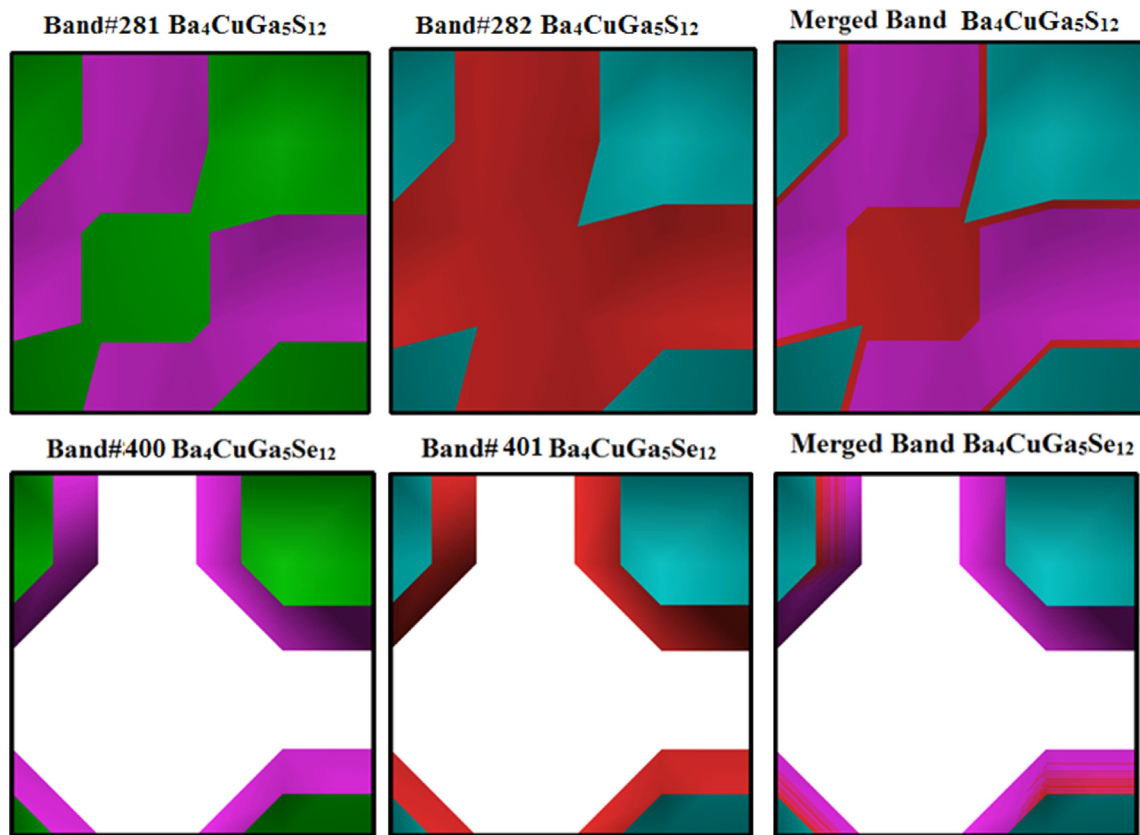


Fig. 5. Calculated Fermi surface for $\text{Ba}_4\text{CuGa}_5\text{S}_{12}$ and $\text{Ba}_4\text{CuGa}_5\text{Se}_{12}$ compounds.

measured thermoelectric properties. When the temperature increases the electrical conductivity of $\text{Ba}_4\text{CuGa}_5\text{S}_{12}$ compound is decreasing while for $\text{Ba}_4\text{CuGa}_5\text{Se}_{12}$ the electrical conductivity is increasing.

We also calculated the temperature-dependent average Seebeck coefficients for variable temperature of $\text{Ba}_4\text{CuGa}_5\text{S}_{12}$ and $\text{Ba}_4\text{CuGa}_5\text{Se}_{12}$ as plotted in Fig. 8b. The room temperature the average Seebeck coefficients shows positive values but when we increase the temperature the average value of Seebeck coefficients come negative. When we change S by Se the whole average value of Seebeck coefficients is negative in the investigated temperature range, signifying that electron-type carriers dominate the heat transport in these materials. This confirm that the investigated materials are good transport materials. The Seebeck coefficients data exhibit a linear decrease behavior with increasing temperature in $\text{Ba}_4\text{CuGa}_5\text{S}_{12}$ material, while the $\text{Ba}_4\text{CuGa}_5\text{Se}_{12}$ shows a linear increase. These variations of the Seebeck coefficient are consistent with the electrical resistivity variations. Both samples have a rather different temperature dependent Seebeck coefficient. In the high-temperature regime, the Seebeck coefficients show quasilinear behavior with temperature, indicative of metallic character. Thus, one can try to extract the value of E_F through the classical formula $S = \pi^2 k_B^2 T / 2eE_F$ assuming a one-band model with an energy-independent relaxation time.

The results of the average thermal conductivity measurements are shown in Fig. 8c. At room temperature, the thermal conductivity values for these materials are very less. At low temperatures, κ increases with temperature and a maximum appears at around 800 K. This is a typical feature for the reduction of thermal scattering at lower temperatures. The maximum takes place at the temperature where the phonon mean free path is approximately equal to the crystal site distance. In Fig. 8c, we show the observed thermal conductivity (k) for both studied materials. The

temperature characteristic of thermal conductivity k of $\text{Ba}_4\text{CuGa}_5\text{S}_{12}$ and $\text{Ba}_4\text{CuGa}_5\text{Se}_{12}$ compounds exhibits the most typical features in all measured thermoelectric properties. The k values for $\text{Ba}_4\text{CuGa}_5\text{S}_{12}$ are greater than $\text{Ba}_4\text{CuGa}_5\text{Se}_{12}$. Furthermore, k increases with increasing temperature but do not show a pronounced maximum. The increase of thermal conductivity for $\text{Ba}_4\text{CuGa}_5\text{S}_{12}$ ($\text{Ba}_4\text{CuGa}_5\text{S}_{12}$) above approximately 400 (320) K attributed to the activation of localized phonon states at high temperatures.

The calculated ZT vs. temperature is shown in Fig. 8d, a low value of ZT is 0.0 at 400 K (0.9 at 500 K) for $\text{Ba}_4\text{CuGa}_5\text{S}_{12}$ ($\text{Ba}_4\text{CuGa}_5\text{Se}_{12}$). Such low ZT values for the $\text{Ba}_4\text{CuGa}_5\text{S}_{12}$ ($\text{Ba}_4\text{CuGa}_5\text{Se}_{12}$) system are a consequence of their low Seebeck coefficient and high thermal conductivity. The best ZT value obtained for $\text{Ba}_4\text{CuGa}_5\text{S}_{12}$ is 0.45 at 800 K and for $\text{Ba}_4\text{CuGa}_5\text{Se}_{12}$ is 0.924 at 300 K (Table 1).

5. Conclusions

We have presented a first principles study on the electronic structure and dispersion of optical constants of $\text{Ba}_4\text{CuGa}_5\text{S}_{12}$ and $\text{Ba}_4\text{CuGa}_5\text{Se}_{12}$ compounds. Our results show that in the vicinity of the Fermi energy, the electronic energy bands have S/Se-p and the Ba-s states character. The peaks in the density of states near the Fermi level are mainly due to the S/Se-p and Ba-s states. It is found that replacing S with Se, result that the whole structures are shifted towards higher energies by around 0.7 eV. The dielectric functions, optical conductivity and reflectivity spectra calculated in the energy range 0–14.0 eV exhibit structures arising due to interband transitions from S-p to Ba-s states. It is noticed that the reflectivity is over 68% (60%) $\text{Ba}_4\text{CuGa}_5\text{S}_{12}$ ($\text{Ba}_4\text{CuGa}_5\text{Se}_{12}$) compounds within the energy range studied. This implies that

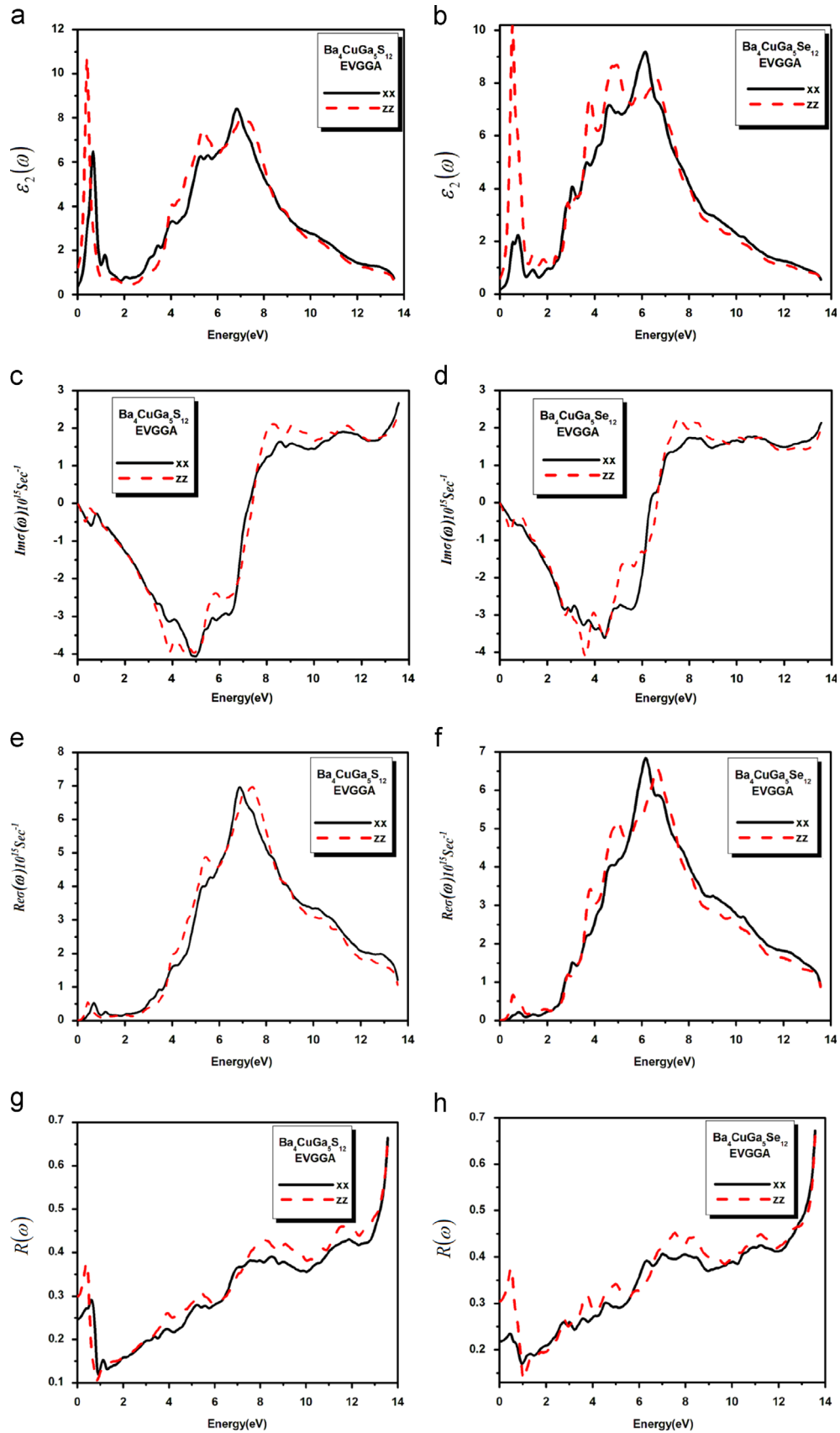


Fig. 6. Calculated; (a and b) imaginary part ($\epsilon_2(\omega)$) of dielectric function; (c and d) imaginary part of the optical conductivity; (e and f) real part of the optical conductivity; (g and h) the reflectivity, for $\text{Ba}_4\text{CuGa}_5\text{S}_{12}$ and $\text{Ba}_4\text{CuGa}_5\text{Se}_{12}$ compounds.

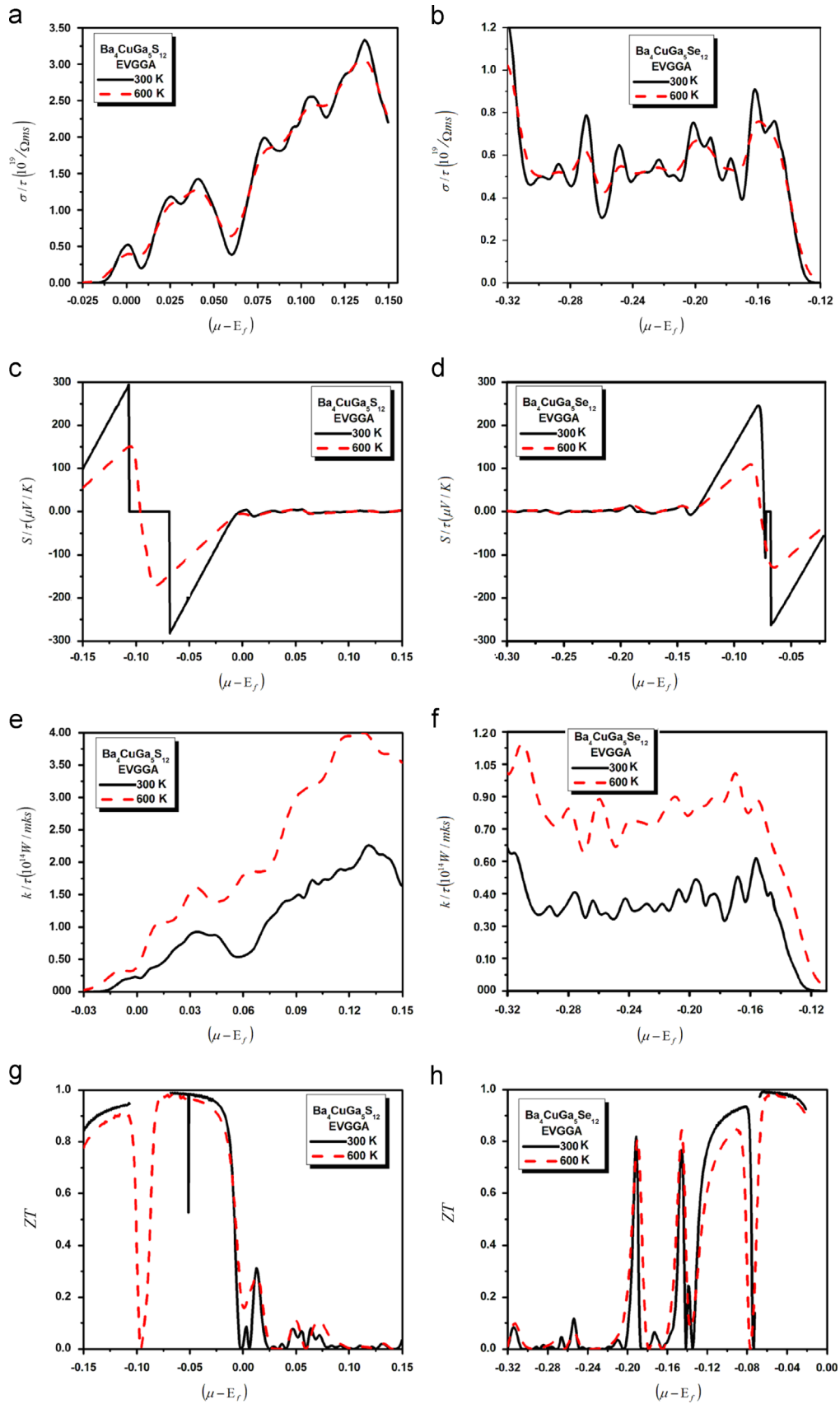


Fig. 7. Calculated thermoelectric properties i.e. Seebeck coefficients, electrical conductivity, thermal conductivity and figure of merit vs. chemical potential.

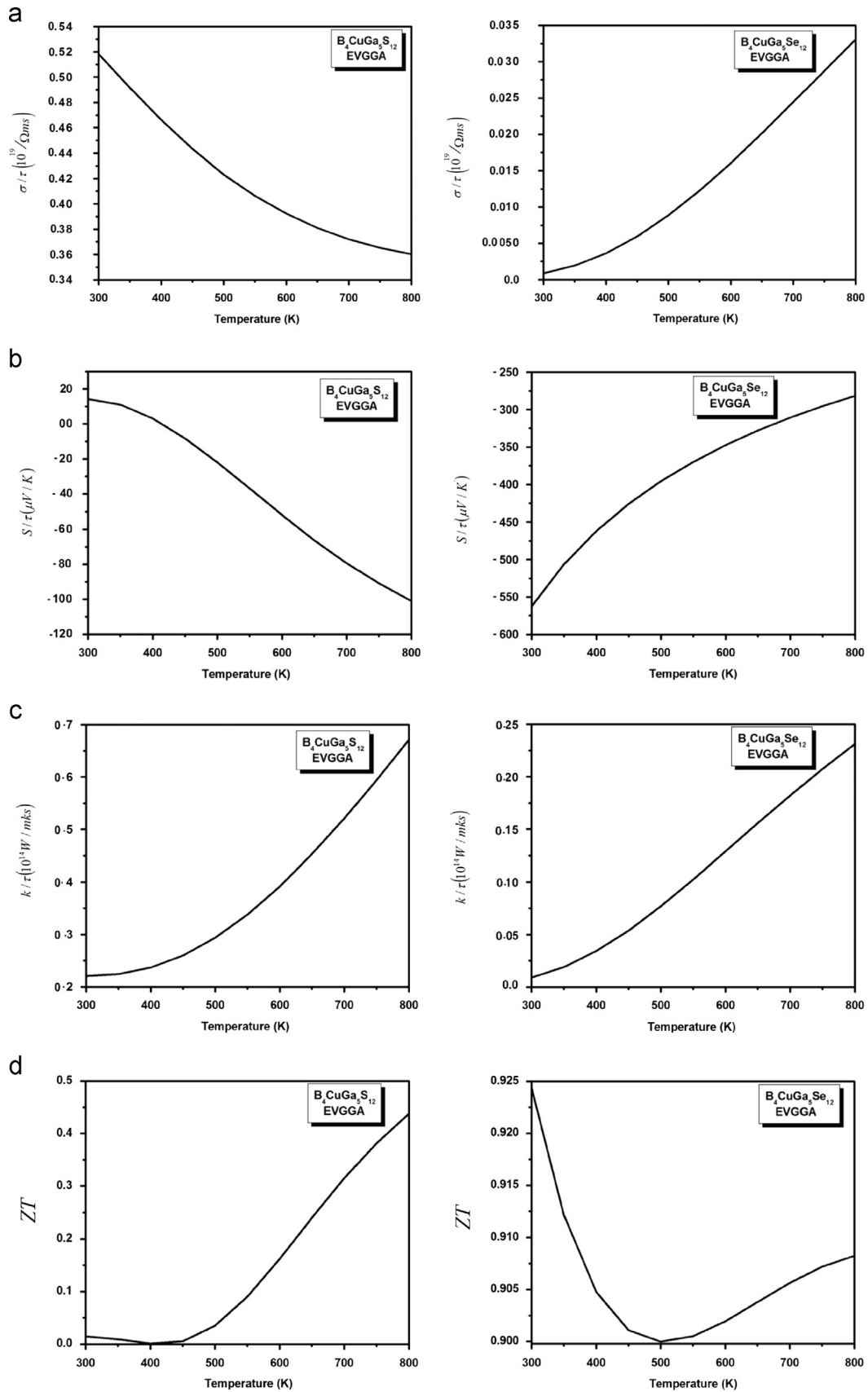


Fig. 8. Calculated thermoelectric properties i.e. Seebeck coefficients, electrical conductivity, thermal conductivity and figure of merit vs. temperatures.

the material will serve as a good reflector. In this work, we also make an attempt by employing the first principles calculations in conjunction with the empirical approaches to predict and interpret the TE properties of the $\text{Ba}_4\text{CuGa}_5\text{S}_{12}$ ($\text{Ba}_4\text{CuGa}_5\text{Se}_{12}$) compounds. We calculated the electronic transport properties of $\text{Ba}_4\text{CuGa}_5\text{S}_{12}$ ($\text{Ba}_4\text{CuGa}_5\text{Se}_{12}$) compounds using BoltzTraP code which employs the semi-classical transport theory and the electronic structures derived from the first-principles calculations. Our work shows that it is possible to predict, at least qualitatively, the TE performance of these $\text{Ba}_4\text{CuGa}_5\text{S}_{12}$ ($\text{Ba}_4\text{CuGa}_5\text{Se}_{12}$) compounds. It may be beneficial to the development of the thermoelectric generators (Table 2).

Acknowledgment

The result was developed within the CENTEM Project, Reg. no. CZ.1.05/2.1.00/03.0088, co-funded by the ERDF as part of the Ministry of Education, Youth and Sports OP RDI programme.

References

- [1] A.H. Reshak, H. Kamarudin, S. Auluck, *J. Phys. Chem. B* 116 (2012) 4677–4683.
- [2] A.H. Reshak, H. Kamarudin, I.V. Kityk, S. Auluck, *J. Phys. Chem. B* 116 (45) (2012) 13338–13343.
- [3] V.G. Dmitriev, G.G. Gurzadyan, D.N. Nikogosyan, *Handbook of Nonlinear Optical Crystals*, Springer, New York, 1999 (references therein).
- [4] P. Becker, *Adv. Mater.* 10 (1998) 979.
- [5] P.S. Halasyamani, K.R. Poeppelmeier, *Chem. Mater.* 10 (1998) 2753.
- [6] C. Chen, Y.J. Wu, *Opt. Soc. Am. B* 6 (1989) 616.
- [7] A.H. Reshak, G. Lakshminarayana, Ya V. Burak, V.T. Adamiv, *J. Alloys Compd.* 509 (2011) 1271–1274.
- [8] C. Chen, B. Wu, A. Jiang, G. You, *Sci. Sin.* B28 (1985) 235.
- [9] L.J. Bromley, A. Guy, D.C. Hanna, *Opt. Commun.* 67 (1988) 316.
- [10] K. Kato, *IEEE J. Quantum Electron.* 27 (1991) 1137.
- [11] A.H. Reshak, I.V. Kityk, S. Auluck, *J. Phys. Chem. B* 114 (50) (2010) 16705–16712.
- [12] R.C. Miller, W.A. Nordland, *Phys. Rev. B* 2 (1970) 4896.
- [13] A.H. Reshak, S. Auluck, M. Piasecki, G.L. Myronchuk, O. Parasyuk, I.V. Kityk, H. Kamarudin, *Spectrochim. Acta Part A: Mol. Biomol. Spectrosc.* 93 (2012) 274–279.
- [14] G.D. Boyd, H.M. Kasper, J.H. McFee, *IEEE J. Quantum Electron.* QE-7 (1971) 563.
- [15] D.C. Hanna, V.V. Rampal, R.C. Smith, *Opt. Commun.* 8 (1973) 151.
- [16] Y.X. Fan, R.C. Eckardt, R.L. Byer, *Appl. Phys. Lett.* 45 (1984) 313.
- [17] P. Canareli, Z. Benko, A.H. Hielscher, R.F. Curl, F.K. Tittel, *IEEE J. Quantum Electron.* 28 (1992) 52.
- [18] P. Canareli, Z. Benko, R.F. Curl, F.K. Tittel, *J. Opt. Soc. Am. B* 9 (1992) 197.
- [19] A. Harasaki, K. Kato, *Jpn. J. Appl. Phys.* 36 (1997) 700.
- [20] B. Tell, H.M. Kasper, *Phys. Rev. B* 4 (1971) 4455.
- [21] G.D. Boyd, H.M. Kasper, J.H. McFee, F.G. Storz, *IEEE J. Quantum Electron.* QE-8 (1972) 900.
- [22] R.L. Byer, M.M. Choy, R.L. Herbst, D.S. Chemla, R.S. Feigelson, *Appl. Phys. Lett.* 24 (1974) 65.
- [23] U. Simon, Z. Benko, M.W. Sigrist, R.F. Curl, F.K. Tittel, *Appl. Opt.* 32 (1993) 6650.
- [24] G.D. Boyd, E. Buehler, F.G.A. Storz, *Appl. Phys. Lett.* 18 (1971) 301.
- [25] G.D. Boyd, T.J. Bridges, C.K.N. Patel, *Appl. Phys. Lett.* 21 (1972) 553.
- [26] R.L. Byer, H. Kildal, R.S. Feigelson, *Appl. Phys. Lett.* 19 (1971) 237.
- [27] A.H. Reshak, H. Kamarudin, S. Auluck, *J. Appl. Phys.* 112 (2012) 053526.
- [28] Y. Kim, S.W. Martin, K.M. Ok, P.S. Halasyamani, *Chem. Mater.* 17 (2005) 2046.
- [29] M.C. Chen, L.M. Wu, H. Lin, L.J. Zhou, L. Chen, *J. Am. Chem. Soc.* 134 (2012) 6058.
- [30] I. Chung, C.D. Malliakas, J.I. Jang, C.G. Canlas, D.P. Weliky, M.G. Kanatzidis, *J. Am. Chem. Soc.* 129 (2007) 14996.
- [31] Y. Kim, I. Seo, S.W. Martin, J. Baek, P.S. Halasyamani, N. Armugam, H. Steinfink, *Chem. Mater.* 20 (2008) 6048.
- [32] I. Chung, J.H. Song, J.I. Jang, A.J. Freeman, J.B. Ketterson, M.G. Kanatzidis, *J. Am. Chem. Soc.* 131 (2009) 2647.
- [33] I. Chung, J.I. Jang, C.D. Malliakas, J.B. Ketterson, M.G. Kanatzidis, *J. Am. Chem. Soc.* 132 (2010) 384.
- [34] M.C. Chen, L.H. Li, Y.B. Chen, L. Chen, *J. Am. Chem. Soc.* 133 (2011) 4617.
- [35] J.H. Liao, G.M. Marking, K.F. Hsu, Y. Matsushita, M.D. Ewbank, R. Borwick, P. Cunningham, M.J. Rosker, M.G. Kanatzidis, *J. Am. Chem. Soc.* 125 (2003) 9484.
- [36] T. Sambrook, C.F. Smura, S.J. Clarke, K.M. Ok, P.S. Halasyamani, *Inorg. Chem.* 46 (2007) 2571.
- [37] I. Chung, J.H. Song, J.I. Jang, A.J. Freeman, M.G.J. Kanatzidis, *Solid State Chem.* 195 (2012) 161.
- [38] J.W. Lekse, M.A. Moreau, K.L. McNerny, J. Yeon, P.S. Halasyamani, J.A. Aitken, *Inorg. Chem.* 48 (2009) 7516.
- [39] X. Lin, G. Zhang, N. Ye, *Cryst. Growth Des.* 9 (2009) 1186.
- [40] J. Yao, D. Mei, L. Bai, Z. Lin, W. Yin, P. Fu, Y. Wu, *Inorg. Chem.* 49 (2010) 9212.
- [41] P. Yu, L.J. Zhou, L. Chen, *Am. Chem. Soc.* 134 (2012) 2227.
- [42] Shu-Ming Kuo, Yu-Ming Chang, In Chung, Joon-Ik Jang, Bo-Hsian Her, Siao-Han Yang, John B. Ketterson, Mercouri G. Kanatzidis, Kuei-Fang Hsu, *Chem. Mater.* 25 (2013) 2427.
- [43] P. Blaha, K. Schwarz, J. Luitz WIEN97, A Full Potential Linearized Augmented Plane Wave Package for Calculating Crystal Properties, Karlheinz Schwarz, Techn. Universit at Wien, Austria, 1999 (3-9501031-0-4).
- [44] J.P. Perdew, A. Zunger, *Phys. Rev. B* 23 (1981) 5048.
- [45] J.P. Perdew, K. Burke, M. Ernzerhof, *Phys. Rev. Lett.* 77 (1996) 3865.
- [46] E. Engel, S.H. Vosko, *Phys. Rev. B* 50 (1994) 10498.
- [47] J.A. Wilson, A.D. Yoffe, *Adv. Phys.* 18 (1969) 193.
- [48] A.H. Reshak, S. Azam, *J. Magn. Magn. Mater.* 342 (2013) 80–86.
- [49] B. Checkerberry, W.E. Pickett, P.B. Allen, *Phys. Rev. B* 14 (1972) 3227.
- [50] A.H. Reshak, S. Azam, *J. Magn. Magn. Mater.* 345 (2013) 294.
- [51] A.H. Reshak, S. Azam, *Int. J. Electrochem. Sci.* 8 (2013) 10396–10423.
- [52] P.M. Chaiken, An introduction to thermopower for those who might want to use it to study organic conductors and superconductors, in: V.Z. Kresin, W. A. Little (Eds.), *Organic Superconductors*, Plenum Press, New York, 1990, pp. 101–105.